CHEMICAL KINETICS
AND CATALYSIS

Effect of the Nature of a Carbon Material on the Kinetics of Carbide Formation in Fe-Containing Catalyst Modified with Copper in CO and Syngas

G. V. Pankina[a],*, P. A. Chernavskii[a], V. O. Kazak[a], N. E. Strokova[a], and V. V. Lunin[a]

[a]*Department of Chemistry, Moscow State University, Moscow, 119991 Russia*
*e-mail: pankina5151@inbox.ru

Abstract—The effect the nature of a carbon material characterized by activated charcoal and sibunit has on the chemical composition and dynamics of activation of Fe-containing catalysts in CO and syngas atmospheres is investigated. It is established that magnetite with $T_\theta = 572$°C forms during the activation of Fe/C$_{act}$ and FeCu/C$_{act}$ in a CO flow; cementite with $T_\theta = 220$°C forms during the activation of Fe/C$_{Sib}$ and FeCu/C$_{Sib}$ in a CO flow; and activation in a CO/H$_2$ flow results in the formation of Hägg carbide χ-Fe$_5$C$_2$ with $T_\theta = 257$°C with all catalysts.

INTRODUCTION

Iron-containing catalysts of Fischer–Tropsch synthesis (FTS) are of interest to researchers due to their high activity and selectivity toward paraffins and olefins. Carbides of different chemical compositions are considered an active phase of Fe-containing catalysts [1]. It is known that modifying Fe-containing catalysts with such metals as copper affects their physicochemical characteristics, activity, and selectivity in the catalytic reaction of CO hydrogenation (FTS). Activation of Fe-containing catalysts in a H$_2$/CO mixture changes their structural and chemical properties and results in the formation of active centers of different chemical composition [2–5]. The authors of [2] thus demonstrated that copper in Fe-deposited catalysts increased the dispersity of the hematite precursor and promoted hydrogen reduction and adsorption, but also suppressed CO adsorption and iron carbidization. In addition, copper in a catalyst's composition increases its selectivity toward light hydrocarbons and methane but reduces its selectivity toward heavy hydrocarbons [2].

Using copper ferrite CuFe$_2$O$_4$ as an example, Van Steen and co-authors showed that introducing copper into the ferrite crystal lattice accelerates the formation of magnetite and metallic Cu in both hydrogen and in CO [3]. Copper increases the conversion of magnetite into α-Fe in a H$_2$ atmosphere, and into Hägg carbide in a CO atmosphere. In addition, the amount of carbide formed under the conditions of the reaction depended on how close the copper and iron were to each other. The authors explained the observed increase in the catalytic activity of copper ferrite by an increase in the specific surface area of the FeC$_x$ carbide phase, where copper played a role of a structural promotor. Copper also facilitated the secondary reaction of olefin hydrogenation. Copper-containing model compounds of the CuFeO$_4$ type demonstrated high CO$_2$ selectivity, which was explained by the presence of small magnetite crystallites in the process of CO hydrogenation.

It was noted in [4] that activation in syngas results in the reduction of Fe$_2$O$_3$ to magnetide and carbidization to FeC$_x$. It was found that the rate and degree of carbidization were much higher when the precursor contained copper additive, which played the role of active centers upon activating the catalysts in CO and H$_2$ [4]. It was suggested that the availability of copper indeed facilitated the formation of carbide seed crystals on the surface of the oxidized iron. The higher the number of seed crystals and the smaller the FeC$_x$ carbide crystallites, the higher the rate of carbidization. These small FeC$_x$ crystallites ensure a large specific surface area and the completeness of Fe$_2$O$_3$ precursor carbidization, thereby guaranteeing high rates of the process [4]. The authors of [6] studied the formation of different carbides such as χ-Fe$_5$C$_2$ and θ-Fe$_3$C during disproportionation on 100-μm iron particles at 500°C in a CO flow.

Using temperature-programmed reduction (TPR) and X-ray diffraction analysis in situ during the reduc-

Table 1. Structural properties of samples (data from low-temperature nitrogen adsorption and XRD)

Sample	$S_{\text{micropore}}$, m^2/g	S_{sp}, m^2/g	$V_{\text{micropore}}$, cm^3/g	d_{av}, Å	D, nm
C_{act}	347	819	0.156	19.7	—
Fe/C_{act}	281	593	0.125	20.1	4.5
Fe/Cu/C_{act}	227	495	0.079	19.4	4.5
C_{Sib}	19.6	408	0.006	48.4	—
Fe/C_{Sib}	30.7	205	0.013	51.3	9.2
FeCu/C_{Sib}	23.5	201	0.009	53.6	9.3

S_{sp} is the specific surface area of the samples (BET data, m^2/g); $S_{\text{micropore}}$ is the specific surface area of micropores in the samples, m^2/g; $V_{\text{micropore}}$ is the specific volume of the samples, cm^3/g; d_{av} is the average size of particles in the samples, Å; D is the size of crystallites (XRD data, nm).

tion of CuCo/SiO$_2$ catalysts, Smith et al. [7] found two forms of intermediates with different degrees of reduction. The adding of copper also resulted in the formation of an easily reduced amorphous fraction of CuO. This proceeded in two consecutive stages: CuO → Cu$_2$O → Cu. The authors of [8] indicated that the promoting role of copper depends largely on the means of catalyst production, e.g., deposition and combined impregnation. The role of copper in the process of carbide formation thus remains a topic of discussion.

The use of different carbon-based materials as supports has attracted considerable attention in recent decades. Compared to oxide supports, they do not interact with active components. They have high specific surface area, exhibit electron conductivity due to the delocalization of π-electrons in graphite crystallites; and are capable of forming carbides [9, 10].

The aim of this work was to investigate the effect the nature of such carbon-based support materials as activated charcoal C_{act} and sibunit C_{Sib} have on the dynamics of carbide formation in Fe-deposited catalysts in the presence of copper during activation in CO and syngas. The physicochemical properties of the catalysts were investigated.

EXPERIMENTAL
Preparing the Catalysts

Our catalysts were produced via triple impregnation of a carbon support using Fe(NO$_3$)$_3$ · 9H$_2$O and Cu(NO$_3$)$_2$ · 6H$_2$O solutions with a copper concentration of 1 wt % and a constant iron concentration of 15 wt % Fe. Activated charcoal C_{act} (VEB Laborchemie Apolda, DDR) and mesoporous composite carbon support sibunit C_{Sib} (Institute of Hydrocarbon Processing Problems, Siberian Branch, Russian Academy of Sciences) were used as supports. Catalysts were dried in a rotary evaporator for 1 h at 80°C, with subsequent calcination in a nitrogen flow (1200 h^{-1}) for 3 h at 450°C with a heating rate 8 K/min. Drying and calcination were repeated after each impregnation.

The resulting catalysts were designated Fe/C_{act}, FeCu/C_{act} and Fe/C_{Sib}, FeCu/C_{Sib}.

Low-Temperature Nitrogen Adsorption

The porous structure of carbon materials (specific surface area, specific surface area of micropores, specific pore volume, average pore size of the samples) and iron/carbon catalysts were examined via low-temperature nitrogen adsorption on a Micromeritics ASAP 2000 instrument. Prior to each experiment, the samples were degassed under vacuum ($P < 10$ mm Hg) at 300°C for 4 h. The obtained results are presented in Table 1.

Determining Elemental Composition

Quantitative determination of the elements (wt %) in the samples was performed through energy-dispersive spectroscopy (EDS) on a JEOL-JSM-6390LA scanning electron microscope. The results from the elemental analysis of the as-prepared samples are presented in Table 2.

X-ray Diffraction Analysis

X-ray diffraction analysis was performed using a DRON-3 diffractometer with CuK_α radiation and a graphite monochromator. Measurements were made in the range 2θ = 20°–70° using the stepwise scanning mode with a step size of 0.1° and exposure time of 3 s per step. To determine the crystallite sizes, scanning was conducted with a step size of 0.02° and 10 s of exposure per step. The average sizes of magnetite crystallites (hkl 311) D were estimated using the Scherrer equation

$$D_{hkl} \approx \frac{\lambda}{\beta \cos \Theta},$$

where λ is wavelength, β is the integral width of a peak at half maximum, and θ is the angle of reflection.

Table 2. Results of elemental analysis of as-prepared samples (wt %)

Sample	Content, wt %										
	C	Fe	Cu	O	Si	S	Cl	Ca	Al	Zn	Mg
C_{act}	81.94	2.1	—	7.8	0.68	0.29	1.87	0.1	0.21	4.89	0.12
Fe/C_{act}	59	21.2	—	13.7	0.6	0.22	1.35	0.17	0.26	3.5	—
$FeCu/C_{act}$	52.73	22	1.06	18.5	0.57	0.15	1.2	0.12	0.41	3.2	0.06
C_{Sib}	97.31	—	—	2.50	—	0.17	—	0.02	—	—	—
Fe/C_{Sib}	74.13	18.97	—	6.77	—	0.13	—	—	—	—	—
$FeCu/C_{Sib}$	72.24	16.87	1.68	9.21	—	—	—	—	—	—	—

Differential Thermal Analysis (DTA/TGA)

Heating was done in an inert atmosphere (argon flow, 80 mL/min) inside a Netzsch STA 449 C Jupiter thermoanalyzer at a rate of 10 K/min in the temperature range of 40 to 600°C. Gases released during heating were analyzed on an Aeolos QMS 403C quadrupole mass spectrometer. Scanning range was $m/z = 10-50$. The following fragments were recorded: H_2O, O_2, CH_3-groups, C, CO_2, CO, NO, N_2, and NO_2.

In situ Magnetometry

Our samples were examined on a vibration magnetometer, using the in situ mode to measure the magnetization of ferromagnetic components that formed during the chemical reaction [11]. Iron, magnetite, and carbide have fairly high magnetic moments that ensure magnetization of the samples. In situ magnetometry is especially informative, as it allows accurate determination of the composition of extremely unstable iron carbides in the process of chemical transformations.

Aliquots of catalysts (20 mg) were reduced in hydrogen, carbon monoxide, or syngas CO/H_2 flows during heating to a temperature of 600°C at a rate of 10 K/min in the measuring cell of a vibration magnetometer. The cell of consisted of a quartz flow-microreactor that allowed the investigation of topochemical transformations in situ [12]. After the set temperature was reached, the catalysts were incubated under isothermal conditions to constant magnetization, indicating completion of the reduction process. Following reduction, the samples were cooled, the flow of reducing gas was replaced with argon and the levels of specific magnetization were measured, depending on temperature (thermomagnetic curve, TMC). The Curie temperatures of the resulting chemical compounds was determined from these dependences.

RESULTS AND DISCUSSION

It was determined from low-temperature nitrogen adsorption that the total pore volume in the activated charcoal was 0.403 cm³/g; in the sibunit, it was 0.409 cm³/g. Analysis of the obtained data (Table 1) showed that the fraction of micropores in the total pore volume of the activated charcoal was 38% ($V_{micropore} = 0.156$ cm³/g), while the fraction of mesopores with an average diameter of 2 nm was 62%. The specific surface area calculated according to BET fell by 140% for the Fe/C_{act} and 170% for the $FeCu/C_{act}$ as the pores filled with iron and copper particles. The volume of micropores dropped from 0.156 to 0.08 cm³/g upon the transformation of C_{act} to $FeCu/C_{act}$, with the specific surface area of micropores shrinking by 150%.

Most of the sibunit C_{Sib} pore volume was localized in mesopores with an average diameter of 4.8 nm, while the fraction of micropores (0.006 cm³/g) in the total volume was only a few percent (Table 1). The specific surface area of Fe/C_{Sib}, calculated according to BET, shrank by 200% (from 408 to 205 m²/g) in comparison to C_{Sib}, but only slightly (to 201 m²/g) for $FeCu/C_{Sib}$. The mesopores and micropores of the supports were thus filled with nanoparticles of the catalyst.

The results from EDS elemental analysis presented in Table 2 show that C_{act} contained admixtures of Fe, Zn, and Mg metals that could affect the physicochemical properties of systems synthesized on their basis. It should be noted that sibunit does not contain any metal impurities. The results presented in Table 2 show that the concentrations of iron in the catalysts were quite different from the ones calculated, while the concentration of copper did not differ from the calculated value. With C_{act}-based catalysts, such a discrepancy can be explained by the support initially containing iron impurities (2.1 wt %). Another explanation has to do with the features of EDS, which allows analysis of the sample surface. The reduction of iron oxide with carbon is also possible during catalyst production (calcination). As indicated below, the temperature of the onset of interaction between iron oxide and carbon, determined for $FeCu/C_{act}$ via TDG/DTA, was 460°C; for $FeCu/C_{Sib}$, it was 350°C. With regard to copper, it was distributed fairly uniformly on the catalyst's surface, and its concentration was virtually the same as the one calculated.

Table 3. Values of temperature maxima (T, °C) for our samples (DTA/TGA data)

Sample	1st peak		2nd peak		3rd peak	
	DTA	TGA	DTA	TGA	DTA	TGA
C_{act}	98.4	103.7	160	260		
C_{Sib}	76	80	—	400		
Fe/C_{act}	111.9	106.3	184.1	210.2		
Fe/C_{Sib}	113.1	117.9	186.7	229.8		
FeCu/C_{act}	114.7	113.4	191.0	206.3	590	320
FeCu/C_{Sib}	79.4	83	350	430	466.4	583.8

A comparison of our catalysts' XRD spectra indicates that the main phase present in all of them was magnetite that formed during their production, which is agrees with the data in [13]. The presence of copper is not indicated in the spectra, due to the low degree of crystallinity and the metal's low concentration.

Thermogravimetric analysis in conjunction with mass spectrometry of the released gases was used to investigate the processes that occur during production of the catalysts. Analysis of the results from DTA/TGA (Table 3) revealed there were two characteristic peaks for all of the investigated catalysts. The first clearly pronounced maximum indicates there was a considerable endothermic effect at $T = 106.3$°C for Fe/C_{act}, at $T = 113.4$°C for FeCu/C_{act}, at $T = 117.9$°C for Fe/C_{Sib}, and at $T = 83$°C for FeCu/C_{Sib}. This effect was most likely due to the removal of the adsorbed and chemically bound water molecules, which was accompanied by mass loss. The second clearly pronounced peak was associated with an exothermic effect at $T = 210.2$°C for Fe/C_{act}, at $T = 206.3$°C for FeCu/C_{act}, at $T = 229.8$°C for Fe/C_{Sib}, and at $T = 430$°C for FeCu/C_{Sib}. This peak was caused by the decomposition of iron nitrate, accompanied by the release of CO_2 and NO and small amounts of N_2 and NO_2 in the case of C_{act}.
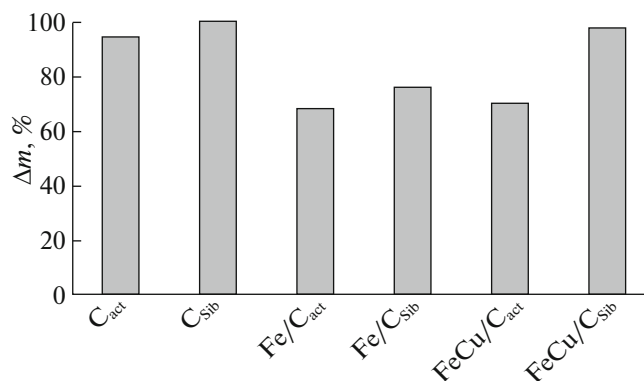
Histogram 1. Residual mass (Δm, %) of the samples after the decomposition reaction (599.9°C).

It is characteristic that the third, slightly pronounced, peak was observed at 320 and 583.8°C for the iron-containing catalysts modified with copper, FeCu/C_{act} for FeCu/C_{Sib}, respectively. The third maximum was associated with the exothermic process of copper nitrate decomposition. The temperature of interaction between iron oxide and carbon in the FeCu/C_{act} system was 460°C. The release of gaseous fragments characteristic of either the removal of carboxyl groups, residual solvent, or nitrogen oxides was observed here (Table 3). The residual mass was 70.3%. The thermal effect ΔH was 775.5 J/g. The temperature of iron oxide interaction for FeCu/C_{Sib} was 350°C, and the presence of copper was likely to slow the release of CO_2, NO, and N_2 considerably, along with the rate of mass loss. The residual mass was 98.2%.

The values of residual masses (%) in the investigated systems are presented in the Histogram 1. Analysis of presented data shows that the mass loss during decomposition of the C_{act} and C_{act}-based iron-containing catalysts was higher than for C_{Sib} and catalysts based on it.

Judging from the peaks' positions, copper in the case of C_{act} inhibited the release of water and activated the process of iron nitrate decomposition. In contrast, copper in the case of C_{Sib} activated the release of water, but greatly inhibited the decomposition of iron nitrate. A comparison of the iron-containing catalysts modified with copper reveals that the release of water occurred more easily with the sibunit support than with activated charcoal (83 and 113°C, respectively), but the process of iron nitrate decomposition was inhibited (430 and 206.3°C, respectively). It is likely that the presence of different additives in the C_{act}-based catalysts (Table 2) activated the process of iron nitrate decomposition. Considering the difference in the temperatures of interaction between iron oxide and carbon, we may assume that under the conditions of the same duration of sample calcination (3 h, 450°C) the size of magnetite particles would be smaller in FeCu/C_{act} (4.5 nm) than in FeCu/C_{Sib} (9 nm), which agrees with the average particle size calculated according to the Scherrer equation (Table 1).

The dynamics of topochemical transformations that occur in iron-containing catalysts was investigated via in situ magnetometry [11].

The dependences of the rate of hydrogen consumption and the change in magnetization during the temperature-programmed heating of the catalyst based on activated charcoal in a 5% H_2/Ar flow are presented in Fig. 1. In [14, 15], we showed that the growth of magnetization depicted in Fig. 1 was due to reduction of hematite to magnetite, and then to metallic iron. The presence of copper lowered the initial temperature of the reduction of hematite to magnetite from 400 to 365°C, and the initial temperature of
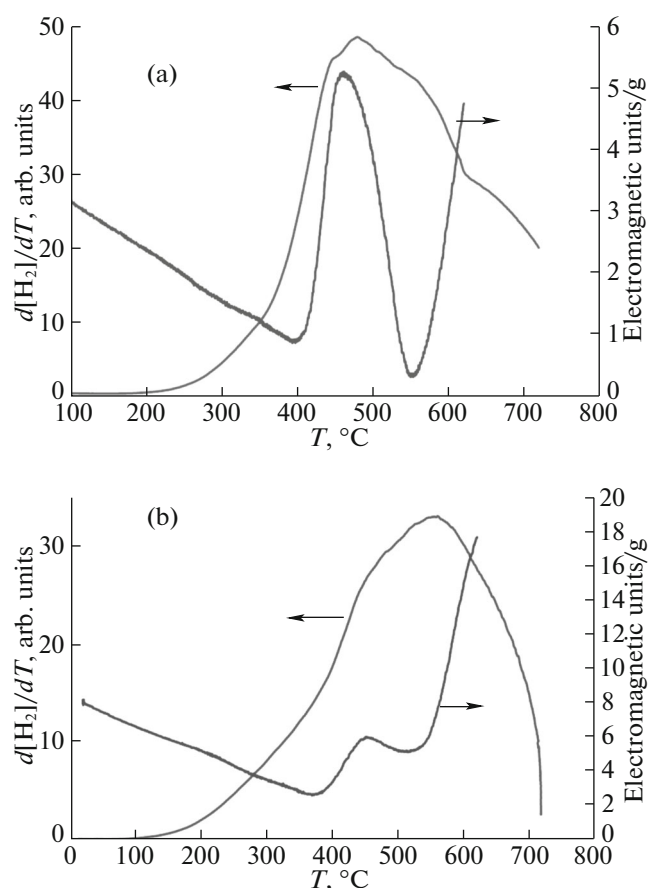
Fig. 1. TPR spectra of Fe-containing catalysts based on activated charcoal in an atmosphere of 5% H_2/Ar: (a) Fe/C_{act}, (b) FeCu/C_{act}.

reduction of magnetite to iron from 545 to 500°C, due to the considerable promoting effect of copper [15].

It should be noted that all of the initial catalyst samples exhibited magnetization, since hematite is partially reduced to magnetite during calcination, a characteristic of Fe/C catalysts as compared to Fe/SiO_2 catalysts [15]. The XRD data corroborate this (Figs. 2a, 2c and 3a, 3c)

The dynamics of the carbidization of Fe/C_{act}, FeCu/C_{act} and Fe/C_{Sib}, FeCu/C_{Sib} in flows of CO and CO/H_2 are presented in Figs. 2a, 2c and 3a, 3c, respectively. The thermomagnetic curves of the catalysts produced by heating them in an Ar atmosphere after prior carbidization are presented in Figs. 2b, 2d and 3b, 3d. For better clarity, the dynamics of the carbidization of Fe/C and FeCu/C_{act} are presented as magnetization vs. time curves in Fig. 3a. This is because FeCu/C_{act} reduction occurs twice as fast as when there is no copper. It follows from the obtained results that adding Cu to Fe/C_{act} has a pronounced promoting effect in a CO/H_2 flow and only a slight effect in a CO flow. It follows from the thermomagnetic curves (TMC, Figs. 2b, 2d and 3b, 3d) that mag-
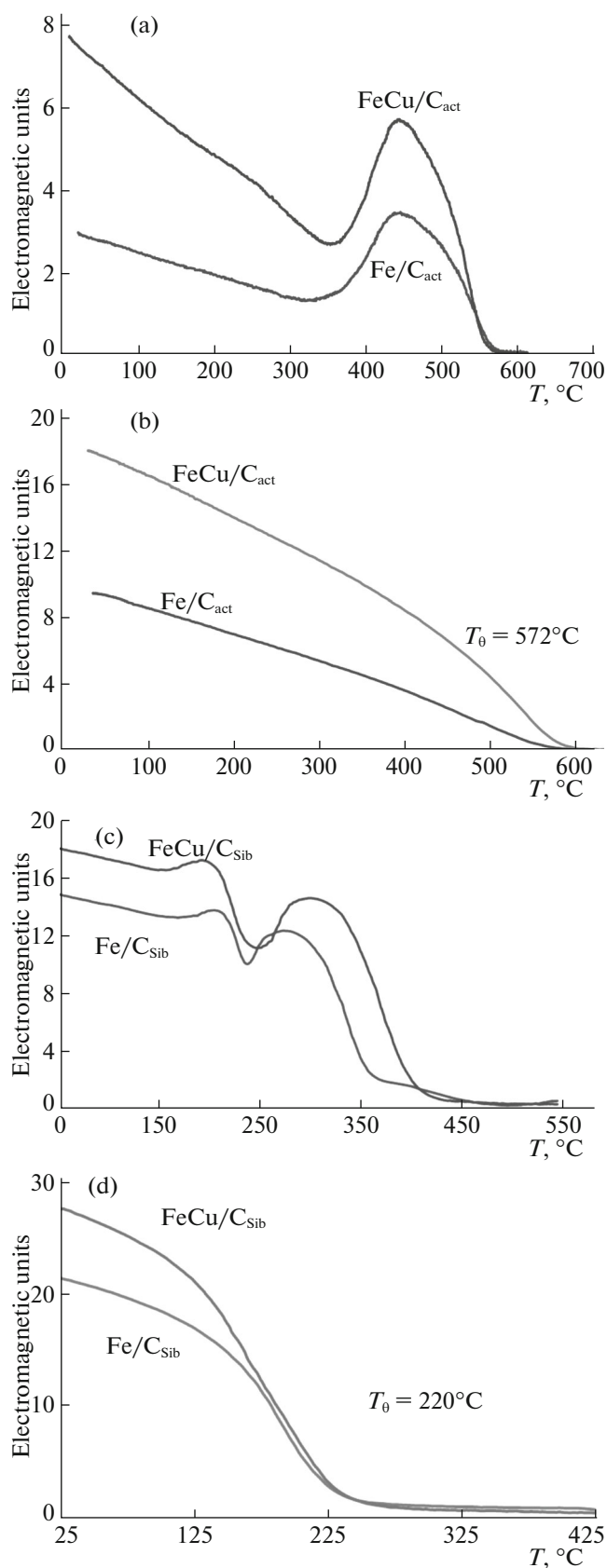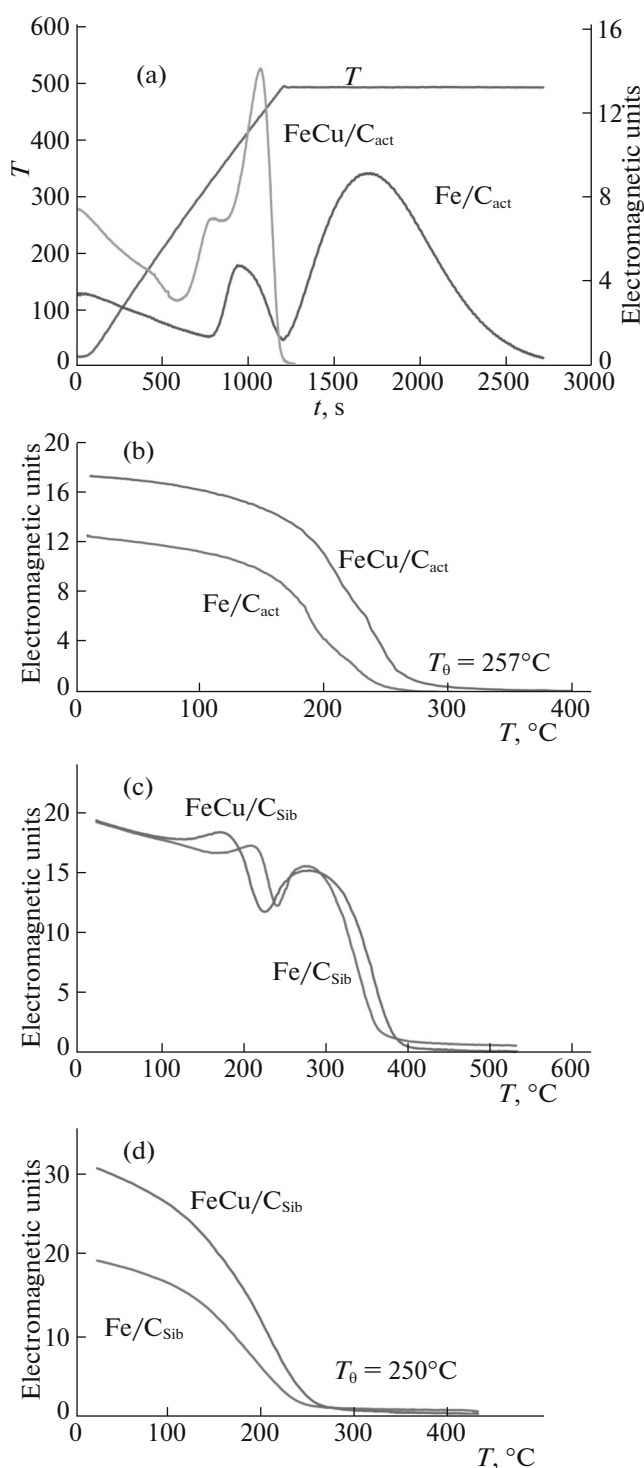

Fig. 2. Dynamics of the carbidization of (a, b) Fe/C_{act}, FeCu/C_{act} and (c, d) Fe/C_{Sib}, FeCu/C_{Sib} in (a, c) a CO flow; (b, d) thermomagnetic curves in an Ar atmosphere.

Fig. 3. Dynamics of the carbidization of (a, b) Fe/C_{act}, FeCu/C_{act} and (c, d) Fe/C_{Sib}, FeCu/C_{Sib} in (a, c) a CO/H_2 flow; (b, d) thermomagnetic curves in an Ar atmosphere. Line T shows the magnetization–time dependence.

netite forms in a CO flow, while Hägg carbide χ-Fe_5C_2 forms in a syngas flow. We can see from the TMC that magnetite is the product formed during the reduction of Fe/C_{act} and FeCu/C_{act} at temperatures of up to $T =$
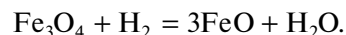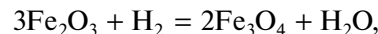
410°C in a CO flow (the maximum peak in Figs. 2a, 2c) and during subsequent cooling. It was therefore established that magnetite is predominately formed for Fe/C_{act} in a CO flow according to the reaction

$$3Fe_2O_3 + CO = 2Fe_3O_4 + CO_2,$$
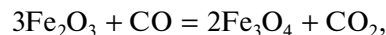
while Hägg carbide χ-Fe_5C_2 is formed predominately in a CO/H_2 flow according to the reaction

$$3Fe_2O_3 = 2Fe_3O_4 + CO_2,$$

$$5Fe_3O_4 + 32CO = 3Fe_5C_2 + 26CO_2.$$
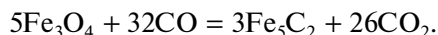
The following processes are also possible in CO/H_2:

$$3Fe_2O_3 + H_2 = 2Fe_3O_4 + H_2O,$$

$$Fe_3O_4 + H_2 = 3FeO + H_2O.$$

With regard to Fe/C_{Sib}, the spectrum displays two characteristic peaks, both during activation in CO and in CO/H_2. The first peak is associated with the reduction of an additional amount of hematite to magnetite. The second peak is related to the transformation of magnetite into carbide. Modifying the Fe/C_{Sib} with copper had no noticeable effect on reduction in CO, but it did increase the amount of formed carbide. The values of specific magnetization of the samples following activation in CO and CO/H_2 flows are presented in Table 4, along with the chemical composition of the product following carbidization.

Cementite θ-Fe_3C with $T_θ = 220°C$ (Fig. 2d) formed with both Fe/C_{Sib} and FeCu/C_{Sib} during carbidization in a CO flow. The presence of copper during the activation of Fe/C_{Sib} in CO/H_2 flow affected the reduction of hematite into magnetite (Fig. 3a), since with Cu there was presumably a spill-over of hydrogen into the composition of syngas.

Analysis of data presented in Table 4 and the values of specific magnetization (Figs. 2b, 2d and 3b, 3d) show that adding copper to all catalysts increased the amount of formed product: magnetite in the case of FeCu/C_{act} in a CO flow (200%) and Hägg carbide in the case of FeCu/C_{Sib} in a CO/H_2 flow (170%). The strong promoting effect of copper was thus demonstrated for FeCu/C_{Sib} in syngas and for FeCu/C_{act} in a CO flow. As follows from Table 4, the largest amount of carbide formed in copper-free samples was observed for the C_{Sib}-based catalyst in a CO flow (19.5), and for the C_{act}-based catalyst in a CO/H_2 flow (12.5).

The processes that occur during activation can thus be represented by the scheme

$$Fe/C + CO \rightarrow Fe_3O_4,$$

$$FeCu/C_{act} + CO/H_2 \rightarrow χ\text{-}Fe_5C_2,$$

$$Fe/C_{Sib} + CO \rightarrow θ\text{-}Fe_3C,$$

$$FeCu/C_{Sib} + CO/H_2 \rightarrow χ\text{-}Fe_5C_2.$$

Table 4. Specific magnetization of catalysts after activation in CO and syngas (electromagnetic units/g)

Catalyst	CO	CO/H$_2$
Fe/C$_{act}$	9.2 (Fe$_3$O$_4$)	12.5 (χ-Fe$_5$C$_2$)
Fe/C$_{Sib}$	19.5(θ-Fe$_3$C)	17.3 (χ-Fe$_5$C$_2$)
FeCu/C$_{act}$	22.0 (Fe$_3$O$_4$)	19.1 (χ-Fe$_5$C$_2$)
FeCu/C$_{Sib}$	27.2 (θ-Fe$_3$C)	31.2 (χ-Fe$_5$C$_2$)

CONCLUSIONS

The nature of carbon material affects the chemical composition of the resulting products, carbides in particular, during the activation of Fe-containing catalysts in a CO atmosphere. The presence of copper does not affect the composition of carbidization products, but it greatly promotes their formation. Fe$_3$O$_4$ with $T_\theta = 572$°C forms during the activation of Fe/C$_{act}$ and FeCu/C$_{act}$ in a CO flow; and cementite θ-Fe$_3$C with $T_\theta = 220$°C forms during the activation of Fe/C$_{Sib}$ and FeCu/C$_{Sib}$ in a CO flow. Hägg carbide χ-Fe$_5$C$_2$ with $T_\theta = 257$°C is the product of the activation of all our catalysts in a CO/H$_2$ flow, and the nature of the carbon material does not affect the composition of the product. The presence of H$_2$ is likely to result in the formation of wustite, which is in turn easily carbidized to Hägg carbide χ-Fe$_5$C$_2$.

ACKNOWLEDGMENTS

REFERENCES

1. M. E. Dry, *Studies in Surface Science and Catalysis* (Elseveier, Amsterdam, 2004), p. 533.
2. H. Wan, B. Wu, Ch. Zhang, H. Xiang, and Y.-W. Li, J. Mol. Catal. A: Chem. **283**, 33 (2008).
3. Z. H. Chonco, L. Lodya, M. Claeys, and E. van Steen, J. Catal. **308**, 363 (2013).
4. S. Li, G. D. Meitzner, and E. Iglesia, J. Phys. Chem. B **105**, 5743 (2001).
5. E. de Smit, A. M. Beale, S. Nikitenko, and B. M. Weckhuysen, J. Catal. **262**, 244 (2009).
6. M. Audier, P. Bowen, and W. Jones, J. Cryst. Growth **64**, 291 (1983).
7. M. L. Smith, A. Campos, and J. J. Spivey, Catal. Today **182**, 60 (2012).
8. E. de Smith, F. M. de Groot, R. Blume, et al., Phys. Chem. A **12**, 667 (2010).
9. C.-m. Li, I. Sayaka, F. Chisato, et al., Appl. Catal. A: Gen. **509**, 123 (2016).
10. J. M. Martin-Martinez and M. A. Vannice, Ind. Eng. Chem. Res. **30**, 2263 (1991).
11. P. A. Chernavskii, G. V. Pankina, and V. V. Lunin, Russ. Chem. Rev. **80**, 579 (2011).
12. P. A. Chernavskii, B. S. Lunin, G. V. Pankina, R. A. Zakharyan, and N. S. Perov, Instrum. Exp. Tech. **57**, 78 (2014).
13. V. V. Ordomsky, K. Cheng, M. Virginie, et al., Appl. Catal. A **488**, 66 (2014).
14. P. A. Chernavskii, V. O. Kazak, G. V. Pankina, et al., ChemCatChem **8**, 390 (2016).
15. V. O. Kazak, G. V. Pankina, P. A. Chernavskii, and V. V. Lunin, Russ. J. Phys. Chem. A **91**, 822 (2017).
16. H. L. Fridman, J. Polym. Sci. C **6**, 183 (1964).

Translated by L. Brovko